

## TOPICAL REVIEW

# Polydiacetylene films: a review of recent investigations into chromogenic transitions and nanomechanical properties

Robert W Carpick<sup>1</sup>, Darryl Y Sasaki<sup>2</sup>, Matthew S Marcus<sup>3</sup>,  
M A Eriksson<sup>3</sup> and Alan R Burns<sup>2</sup>

<sup>1</sup> Engineering Physics Department, University of Wisconsin—Madison, Madison, WI 53704, USA

<sup>2</sup> Biomolecular Materials and Interfaces Department, Sandia National Laboratories, Albuquerque, NM 87185, USA

<sup>3</sup> Physics Department, University of Wisconsin—Madison, Madison, WI 53704, USA

Received 18 February 2004

Published 28 May 2004

Online at [stacks.iop.org/JPhysCM/16/R679](http://stacks.iop.org/JPhysCM/16/R679)

DOI: 10.1088/0953-8984/16/23/R01

## Abstract

Polydiacetylenes (PDAs) form a unique class of polymeric materials that couple highly aligned and conjugated backbones with tailorable pendant side-groups and terminal functionalities. They can be structured in the form of bulk materials, multilayer and monolayer films, polymerized vesicles, and even incorporated into inorganic host matrices to form nanocomposites. The resulting materials exhibit an array of spectacular properties, beginning most notably with dramatic chromogenic transitions that can be activated optically, thermally, chemically, and mechanically. Recent studies have shown that these transitions can even be controlled and observed at the nanometre scale. These transitions have been harnessed for the purpose of chemical and biomolecular sensors, and on a more fundamental level have led to new insights regarding chromogenic phenomena in polymers. Other recent studies have explored how the strong structural anisotropy that these materials possess leads to anisotropic nanomechanical behaviour. These recent advances suggest that PDAs could be considered as a potential component in nanostructured devices due to the large number of tunable properties. In this paper, we provide a succinct review of the latest insights and applications involving PDA. We then focus in more detail on our work concerning ultrathin films, specifically structural properties, mechanochromism, thermochromism, and in-plane mechanical anisotropy of PDA monolayers. Atomic force microscopy (AFM) and fluorescence microscopy confirm that films 1–3 monolayers thick can be organized into highly ordered domains, with the conjugated backbones parallel to the substrate. The number of stable layers is controlled by the head-group functionality. Local mechanical stress applied by AFM and near-field optical probes induces the chromogenic transition in the film at the nanometre scale. The transition

involves substantial optical and structural changes in a highly compressed form. Thermochromism is also studied using spectroscopic ellipsometry and fluorescence intensity measurements, and reveals that ultrathin films can reversibly attain an intermediate phase before irreversibly transforming to a final stable state. Further AFM studies also reveal the relation between the highly anisotropic film structure and its nanomechanical properties. In particular, friction at the nanometre scale depends dramatically upon the angle between the polymer backbone and the sliding direction, with the maximum found when sliding perpendicular to the backbones. The observed threefold anisotropy in mechanical dissipation also leads to contrast in the phase response of intermittent-contact AFM, indicating for the first time that in-plane anisotropy of polymeric systems in general can be investigated using this technique.

## Contents

1. Introduction	680
2. Essential properties of polydiacetylenes and their transitions	681
3. Recent progress in the study of ultrathin PDA films	683
3.1. Preparation of high-quality films	684
3.2. Instrumentation	685
3.3. Film structure	685
3.4. Mechanochromism	686
3.5. Thermochromism	688
3.6. Friction anisotropy	691
3.7. Imaging in-plane anisotropy with intermittent-contact AFM	692
4. Conclusions	694
Acknowledgments	695
References	695

## 1. Introduction

Materials that change in response to external stimuli are of widespread fundamental interest due to the fascinating and complex nature of coupled material responses, such as molecular structure and optical or mechanical properties. The intense level of interest in nanotechnology has added to the excitement surrounding such materials due to the possibility of fabricating dense arrays of nanodevices with built-in and measurable sensitivity to environmental conditions. Rapid sensing of dangerous biological agents [1–3], micro- or nano-fluidic devices [4] or highly dense information storage [5] are notable applications. Polydiacetylenes (PDAs) [6] merit particular interest as these molecules exhibit strong optical absorption and fluorescence emission that change dramatically with various stimuli, namely optical exposure (*photochromism*) [7–10], heat (*thermochromism*) [11–15], applied stress (*mechanochromism*) [10, 16–18], changes in chemical environment [19, 20], and binding of specific chemical or biological targets to functionalized PDA side-chains (*affinochromism/biochromism*) [1–3]. These chromogenic transitions, along with other properties such as high third-order nonlinear susceptibility, unique photo-conduction characteristics, and strong nanometre-scale friction anisotropy [21], render PDA a uniquely interesting material.

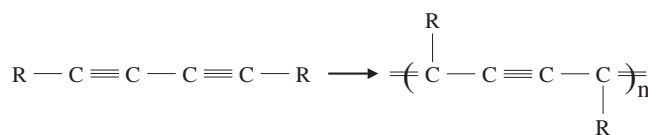


**Figure 1.** Monomeric (left) and polymerized form of the diacetylene, where R represents the pendant side-groups.

In this paper, we briefly review the essential properties of polydiacetylenes and then summarize a broad range of recent results that highlight the latest insights into their fascinating properties and applications. We then focus on our own work that has been dedicated to the study of ultrathin PDA films formed via Langmuir deposition, and the subsequent measurement of their structural, optical, and mechanical properties at the nanometre scale. By altering the head-group functionality, we can choose between mono- and tri-layer PDA film structures. We then show that we can use the tip of an atomic force microscope (AFM) or a near-field scanning optical microscope (NSOM) tip to locally convert the PDA from the blue form to the red form via applied stress. This represents the first time that mechanochromism has been observed at the nanometre scale. Dramatic structural changes are associated with this mechanochromic transition and include the observation of a highly distorted, condensed state. Thermochromism is also studied using spectroscopic ellipsometry and fluorescence intensity measurements, and reveals that ultrathin films can reversibly attain an intermediate phase before irreversibly transforming to a final stable state. Further AFM measurements also reveal strongly anisotropic friction properties that are correlated with the orientation of the conjugated polymer backbone. The threefold contrast in friction and the associated mechanical anisotropy produces unexpected contrast in intermittent-contact atomic force microscopy (IC-AFM). In IC-AFM, the cantilever tilt breaks the tip-sample rotational symmetry and enables measurements of in-plane anisotropic forces. The anisotropic forces result in varying energy dissipation depending on the cantilever-sample orientation, yielding phase contrast. The unique anisotropic properties of PDA have therefore allowed us to demonstrate very generally that in-plane properties, as opposed to the commonly discussed out-of-plane properties, can be measured with IC-AFM. We then conclude with suggestions for future research efforts and applications involving PDA.

## 2. Essential properties of polydiacetylenes and their transitions

The properties of PDAs were reviewed in 1985 by Bloor [6]. Substantial interest in PDAs has ensued since then, and a wide array of research efforts have uncovered new properties and insights. The forms in which PDAs can be structured are numerous: bulk single crystals [6], multilayer films [22, 23], monolayer films in both the Langmuir [23] and self-assembled [24, 25] form, vesicles suspended in liquids [2, 20], and as nanocomposite components integrated into inorganic host matrices [26].

Properties of substantial interest include their high nonlinear optical susceptibility [27], ultrafast optical response [28], and strong structural anisotropy imposed by the highly aligned, linear backbones. However, the most deeply investigated aspect of PDAs are the chromogenic transitions they exhibit.

Generally speaking, optical absorption in PDAs occurs via a  $\pi$ -to- $\pi^*$  absorption within the linear  $\pi$ -conjugated polymer backbone [6] (figure 1). Unpolymerized films do not exhibit absorption in the visible region. Upon polymerization, frequently the first chromogenically

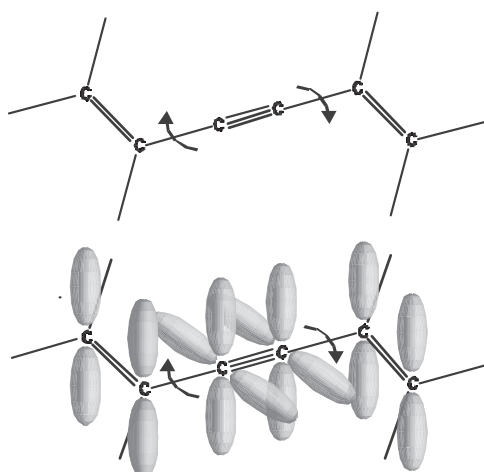


**Figure 2.** Schematic diagram of the molecular orbitals in the  $\pi$ -conjugated PDA backbone in the planar configuration. Energy levels are affected by the overlap of these orbitals. This overlap is altered by rotation about one of the C–C bonds in the backbone. The red phase may consist of a non-planar backbone configuration in conjunction with rotated and/or distorted alkyl side-chains.

interesting state of the PDA appears blue in colour, with an absorption maximum in the range of  $\sim 640$  nm, although other features including a prominent vibronic side-peak are readily apparent. The chromogenic transitions listed in the introduction all involve a significant shift in absorption from low- to high-energy bands of the visible spectrum, where the PDA transforms from a blue to a red colour, with an absorption maximum in the range of  $\sim 540$  nm. In the case of thermochromism, the change is understood to be a first-order phase transition and tends to occur in the range of  $120$ – $150$  °C. The specifics of the absorption spectrum, transition temperature, and so forth vary somewhat with the nature of the pendant side-groups and the form of the PDA (bulk crystal, film, vesicle, etc).

In addition, the red phase tends to exhibit strong fluorescence, while the blue phase does not. This is believed to be due to energy shifts in the lowest-lying excited states [29] such that the very lowest excited state in the blue form has the same symmetry as the ground state ( $A_g$ ), a dipole-forbidden transition. In the red form, this lowest excited state has  $B_u$  symmetry, allowing radiative decay. Strong fluorescence, typically peaked at  $\sim 650$  nm, is thus observed for the red form [10].

The mechanism behind these transitions is not fully established. Previously, a number of other mechanisms attempting to explain the transition had been suggested, and are briefly reviewed by Lee *et al* [15]. For example, it was proposed that the chromatic transition involved a transformation from the ene-yne structure to a butatrienic structure (three sequential double bonds) [13, 30]. However, this has been ruled out by crystallographic studies and quantum chemical calculations [31]. Recent investigations have produced new and detailed insights on both bulk and thin-film forms of PDA. The picture that has emerged from these studies is that the key to the transition is the interplay between the conformation of the pendant side-groups and the backbone [32]. The absorption properties of the backbone depend sensitively on strain. In particular, rotation about the C–C bond of the polymer backbone, which changes the planarity of the backbone, is critical (figure 2). Theoretical calculations indicate that a rotation of only a few degrees about this bond dramatically changes the  $\pi$ -orbital overlap [33–35], causing a significant blue-shift of the absorption spectrum.

Rotation about this bond necessitates changes in the conformation of the pendant side-groups, and thus there exists a sensitive interplay between them. The side-groups will have a preferred packing arrangement which dominates the intermolecular arrangement in the unpolymerized form. This packing arrangement may be dictated by H-bonding between urethane groups, for example [15], or simply due to the substantial van der Waals' interaction between lengthy alkyl chains [36, 37]. During the polymerization, the extended backbones will form in a strained configuration because of the geometric restriction imposed by the side-group arrangement. Essentially, the packing energy of the side-groups creates a barrier that prevents the backbone from adopting a more relaxed form. The subsequent application of heat, stress, or other stimuli leads to side-chain fluctuations or reconfigurations and allows the backbone to adopt a more relaxed conformation that involves rotation about the C–C backbone bonds, and thus leads to changes in the optical absorption spectrum. In the absence of the pendant side-groups, there would be, hypothetically, a monotonic and reversible change in the energy of the polymer backbone as the C–C bond angle changes [33, 38]. The torsional mobility of the polymer backbone is restricted by pendant side-group interactions as well as interactions between the head-groups [38]. The degree of reversibility of the transition likely depends on the height of the energy barrier and the total energy difference between the two conformations.

The evidence for this mechanism is provided in recent NMR studies by Tanaka *et al* [39], Lee *et al* [15], and Cholli and Sandman [40], and FTIR data of Lio *et al* [12] and Rubner *et al* [41]. The recent results from Lee *et al* for thermochromic transitions of urethane-substituted side-groups are particularly convincing as they involve a detailed comparison using NMR and FTIR between thermochromic and nonthermochromic forms of PDA, as well as a comparison between different side-groups. In summary, they show that mechanical strain in the backbone is released in the red phase, and this is accompanied by a change in the conformation of particular C atoms in the pendant side-groups. They also show that PDAs with side-groups that are more restricted show better reversibility, consistent with the notion expressed above that reversibility is a function of the conformational energy difference between the blue and red phases.

Most studies of PDA transitions have focused on thermochromism. Mechanochromism has only been observed in a few instances, initially only at macroscopic scales. Müller and Eckhardt observed an irreversible transition in a PDA single crystal induced by compressive stress [16], which resulted in coexisting blue and red phases. Nallicheri and Rubner [17] observed reversible mechanochromism for conjugated PDA chains embedded in a host elastomer that was subjected to tensile strain. Tomioka *et al* induced reversible chromism by varying the lateral surface pressure of a PDA monolayer on the surface of water in a Langmuir–Blodgett trough [18], with the red form present at higher (compressive) surface pressures. These macroscopic studies of mechanochromism have so far not examined molecular-level structural changes associated with the observed transitions. Our work, discussed below, revealed the first nanometre-scale observations of mechanochromism in PDAs.

One of the other unusual properties of polydiacetylenes is that the photopolymerization occurs via topochemical polymerization from a well ordered solid state, leading to extremely linear, aligned polymerized domains. Crystalline packing of the monomers is required, and the polymerization successfully proceeds because the monomer spacing, imposed primarily by the van der Waals' forces between the pendant alkyl chains, is fortuitously close to the spacing required for the diacetylene backbone to form (figure 3). This 'correct' monomeric spacing refers in particular to the spacing of monomers that are 'nested' with their neighbours via the kink imposed by the diacetylene group. Thus, polymerization is strongly preferred along this direction only, leading to highly linear backbones. The importance of this spacing was highlighted by Mowery *et al*, by showing that the polymerization of diacetylene monolayer films is readily disrupted by atomic-scale roughness of the substrate [25, 42].

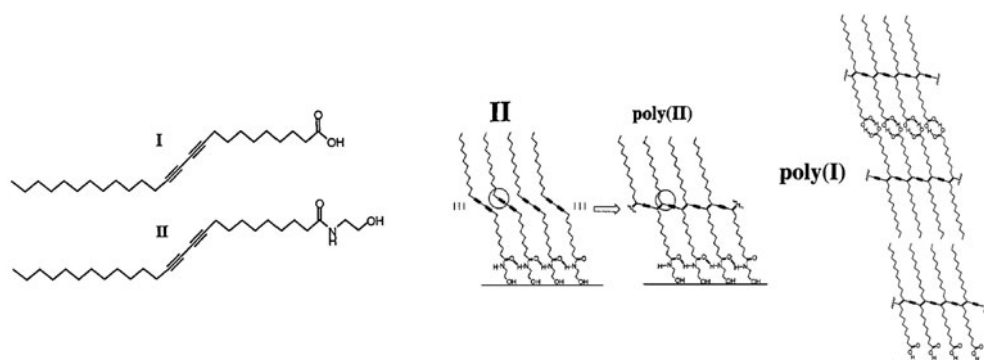


**Figure 3.** Left: PCDA (I) and PCEA (II) molecules. Middle: schematic diagram of molecular orientation of II and its subsequent conversion to poly(II) upon UV irradiation. A hydrogen-bonded network at the headgroup position in the monolayer is drawn. Right: poly(I) in its trilayer form. Hydrogen-bonded carboxylate dimers bind the top two layers to each other, and the lowest layer is bonded to the substrate through hydrogen bonds. van der Waals' interactions bond the lowest and middle layers.

The applications for PDAs are numerous, particularly in the area of sensors. These have yet to see widespread commercial implementation but numerous patents have certainly been filed and work to develop these systems is ongoing. Several groups, starting with Charych *et al*, have produced a substantial body of work demonstrating the use of PDAs as specific colorimetric detectors of biological interactions [1–3]. Other applications are found in photonics, due to their large third-order nonlinear susceptibility and ultrafast response [27]. Examples include optical limiters [43], phase modulators and waveguides [44–46], single-photon tunnelling devices [47], and optically based strain measurements [48, 49]. Use of PDA monolayers as a resist material for microfabrication has also recently been demonstrated [50].

### 3. Recent progress in the study of ultrathin PDA films

We now review recent work of ours involving monolayer and trilayer PDA films produced using Langmuir techniques. As pointed out above, such ultrathin films are of interest because of their potential applications in micro- and nano-devices, as colorimetric sensing surfaces, and for fundamental studies using surface-sensitive probes including scanning probe microscopy.

#### 3.1. Preparation of high-quality films

We have found that Langmuir techniques, where monomers are spread onto a water surface, compressed, and then polymerized *before* deposition onto a substrate, are extremely effective in producing well controlled, highly organized ultrathin PDA films. Details of our materials and sample preparation are described elsewhere [23]. Briefly, diacetylene molecules with two distinct head-groups were made into separate films (figure 3). The first, 10,12-pentacosadiynoic acid (PCDA) (I) (Farchan/GFS Chemicals), was received as a bluish powder which was purified by recrystallization to remove polymer content. The second molecule, N-(2-ethanol)-10,12-pentacosadiynamide (PCEA) (II), was prepared by coupling ethanolamine with 10,12-pentacosadiynoyl chloride in tetrahydrofuran and triethylamine. The acid chloride was prepared from the PCDA using oxalyl chloride in methylene chloride. PCEA was isolated by flash column chromatography on silica gel (25% ethylacetate/hexanes,  $R_f = 0.23$ ).



Langmuir film preparations were performed on a Langmuir trough (Nima) which was situated on a vibration isolation table inside a class 100 clean room. The pure water subphase was kept at  $15 \pm 0.2^\circ\text{C}$ . Diacetylene monomers were spread on the water surface in a 50% chloroform/benzene solution. This solvent mixture is chosen for improved solubility of PDA and ease of spreading on the water surface. All films were incubated for 10–15 min at zero pressure prior to compression.

For polymerization at the air–water interface, the films were compressed to a surface pressure of  $20 \text{ mN m}^{-1}$ , then equilibrated for 20–30 min. UV irradiation of the compressed films was performed with a pair of pen lamps (Oriel). UV exposure was controlled by setting the lamp height above the air–water interface and choosing specific exposure times as described elsewhere [23]. A few minutes after UV exposure, the water was slowly drained off by aspiration. The films were laid down on mica (freshly cleaved) or silicon (Piranha-cleaned) substrates that were pre-submerged horizontally in the aqueous subphase before monolayer spreading. The substrate was then removed and dried in clean room air. This horizontal transfer method proved to be the most effective for producing high-quality films, as polymerization creates a degree of rigidity in the film on the water surface. This rigidity renders vertical transfer methods unreliable as the films would not uniformly compress during vertical transfer.

### 3.2. Instrumentation

A Nanoscope IIIA AFM (Digital Instruments) operating in contact mode was used to obtain topographic and friction force images. The same type of AFM was used to obtain IC-AFM measurements. Contact-mode AFM data were acquired under laboratory ambient conditions. Silicon nitride cantilevers (Digital Instruments) with a nominal normal force constant of  $0.06 \text{ N m}^{-1}$  were used for all contact-mode measurements. For IC-AFM images, Si cantilevers were used. A novel NSOM custom built at Sandia National Laboratories [51] was used to simultaneously observe sample fluorescence with sub-wavelength lateral spatial resolution, as well as normal forces and shear forces. The tips used were Al-coated etched optical fibres. A variable angle spectroscopic ellipsometer (J A Woollam Co., Lincoln, NE) was employed for ellipsometric studies of the thermochromic transition. Sample temperature during the measurements is controlled with a small home-built heat/cool stage. Time-resolved measurements of fluorescence during the thermal transition used an optical platform incorporating a CCD spectrometer with fibre optic collection system. The temperature was controlled with the same heat/cool stage as used for the previous measurements. Poly-PCDA fluorescence was recorded using a fibre-optic-coupled spectrometer (Ocean Optics, Dunedin, FL).

### 3.3. Film structure

Pressure–area isotherms indicate the amphiphiles of **I** and **II** on pure water both had identical take-off areas of  $25 \text{ \AA}^2/\text{molecule}$ , corresponding to the molecular cross-section of the hydrocarbon–diacetylene structure. The film of **I** collapses at low pressure ( $\sim 12 \text{ mN m}^{-1}$ ), but upon over-compression reaches a stable solid phase with a limiting molecular area of  $\sim 8 \text{ \AA}^2/\text{molecule}$ . This over-compressed state corresponds to a stable trilayer structure. The film of **II** was stable as a monolayer with a collapse pressure of about  $35 \text{ mN m}^{-1}$  and an extrapolated molecular area at zero pressure of  $25 \text{ \AA}^2/\text{molecule}$ . After equilibration, films were polymerized to the blue phase by UV exposure at incidence powers of  $40 \text{ \mu W cm}^{-2}$  for **I** and  $23 \text{ \mu W cm}^{-2}$  for **II** over a period of 30 s. Red-phase films were produced by exposing the trilayer of **I** to  $500 \text{ \mu W cm}^{-2}$  and the monolayer of **II** to  $40 \text{ \mu W cm}^{-2}$  for 5 min.

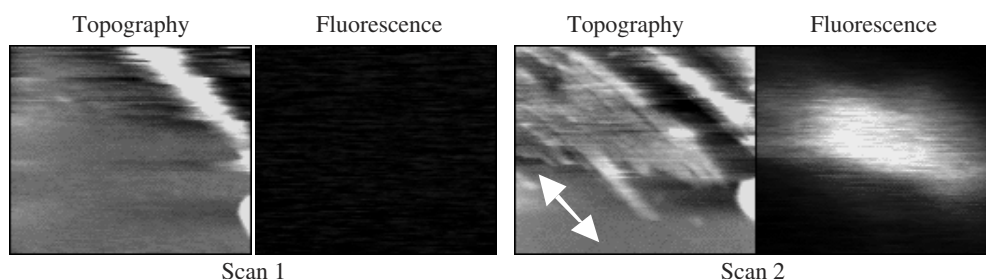


**Figure 4.** NSOM shear force topography and simultaneous fluorescence images ( $2.4 \times 2.4 \mu\text{m}^2$ ) showing tip-induced mechanochromism.

AFM images of the blue- and red-phase forms of poly(**I**) and poly(**II**) on muscovite mica or silicon substrates confirm that the coverage for all films was nearly uniform for the entire substrate. Over 95% of the transferred film was flat to within  $\pm 0.5$  nm, with up to  $100 \mu\text{m}$  crystalline domains observed. AFM measurements confirmed that films of **I** and **II** formed trilayers and monolayers respectively. There were distinct height differences between the blue- and red-phase films of both **I** and **II**. The heights of the blue- and red-phase trilayers of poly(**I**) were measured at  $7.4 \pm 0.8$  and  $9.0 \pm 0.9$  nm, respectively. The blue- and red-phase poly(**II**) monolayer films had similarly proportional height differences of  $2.7 \pm 0.3$  and  $3.1 \pm 0.3$  nm, respectively. The films possess highly aligned striations corresponding to small height variations of  $\sim 2$  Å discussed further below, and similar to previous reports [12]. These striations appear to be small variations in density or side-chain tilt angle and are aligned with the polymer backbone direction, as confirmed with polarized fluorescence microscopy.

These results provide insight into the stabilization of diacetylene films. The head-group interactions and alkyldiyne chain stacking should dominate the film structure of the monomeric diacetylene Langmuir films. The ability of the amide head-group of **II** to form lateral intermolecular hydrogen-bonded structures (figure 3, centre), similar to  $\beta$ -sheets in proteins, may explain the stability of this monolayer film on pure water. In contrast, **I** films on pure water are unstable as monolayers but stack favourably into trilayers. Carboxylic acid dimer formation aids in stabilizing this structure. Indeed, stable bilayer islands are commonly observed on top of the **I** trilayer. Thus, by altering the head-group, we can control whether the resulting film will be structured as a monolayer or a trilayer. Further details of the film preparation and structure are published elsewhere [23].

### 3.4. Mechanochromism

The blue-to-red transition can be activated at the nanometre scale using NSOM or AFM tips on both the trilayer poly(**I**) and monolayer poly(**II**) [10, 52]. Figure 4 shows simultaneous NSOM topography and fluorescence images on a blue poly(**I**) film. In the first scan (left-hand pair), no fluorescence is seen over the flat PCDA region. In the subsequent scan (right-hand pair), topographic changes are created, and localized fluorescence emission is produced. A fluorescence spectrum obtained over this region reveals the spectral fingerprint of red PCDA. These observations were reproducible. In general, when this transition is observed, the fluorescent regions grow in size with each image acquired.

The blue-to-red transition has also been produced using AFM tips with both trilayer poly(**I**) and monolayer poly(**II**) blue films (figure 5). With AFM, local topographic changes, discussed below, are observed *in situ*. These changes indicate the transition is taking place. By creating



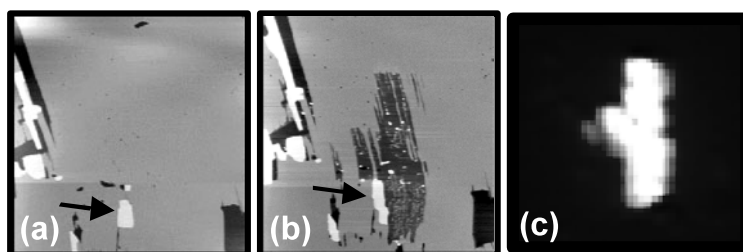


**Figure 5.**  $10 \times 10 \mu\text{m}^2$  topographic AFM images showing tip-induced patterning of red PCDA domains. (a) Initial image of a blue film. (b) Final image with a patterned red region. The backbones are oriented in roughly the vertical direction. The patterning was formed by multiple, high-load scans within the patterned region. The black arrow indicates a bilayer island that has grown in size after patterning. (c) Far-field fluorescence image of the same region. Characteristic red PCDA fluorescence is localized within the patterned region.

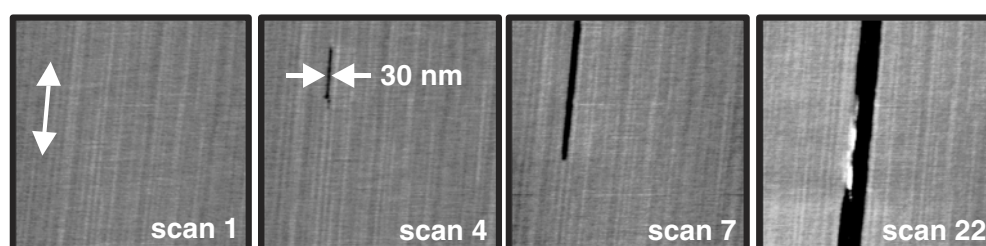


**Figure 6.** Series of  $1 \times 1 \mu\text{m}^2$  topographic AFM images of blue PCDA showing the progressive growth of the tip-induced red domains. In the first scan, striations indicative of the polymer backbone direction are observed. By the fourth scan, a topographically distinct (i.e. lower) region, only 30 nm wide, appears. This region continues to grow in subsequent scans.

a large ( $>1 \mu\text{m}$ ) red region, *ex situ* fluorescence microscopy is used to confirm that a red region has been created by the AFM tip. With both AFM and NSOM, normal forces alone are not sufficient to cause the transition. Shear forces must also be applied, i.e. during the scanning process, to produce the blue-to-red transition. This was ascertained by observing that the transition does not occur when applying high normal loads in the absence of lateral sliding. In all cases, the observed transitions are irreversible up to at least several months.

The transformed region can be as small as 30 nm wide (and perhaps smaller, with the resolution being limited by the finite size of the AFM tip). This is illustrated in the series of topographic AFM images in figure 6, which show the progressive growth of the transformed region. The typical, anisotropic growth is clearly seen, whereby the growth proceeds much more rapidly along the polymer backbone direction.

The transformed regions consistently exhibit higher friction, increased roughness, and a surprising height reduction of typically 40–50% of the original film height. High-resolution images of the transformed regions, however, consistently reveal backbone-related striations. This indicates a substantial degree of preservation of the conjugated backbone despite the dramatic height reduction. No such structural changes for other types of PDA have been previously reported.

While this height reduction could be explained by a removal of one or more layers in the trilayer poly(I) film, this cannot explain the comparable height reduction for the monolayer. One possibility is that some molecules are removed during the transformation process, and the remaining molecules substantially increase the tilt angle of the hydrocarbon side-chains. The

all-*trans* nature of the side-chains may also be strongly disturbed, but the backbone structure remains. This increased tilt angle and conformational changes allow stress within the backbone and side-chains to be relieved as discussed below. This picture is consistent with the observation via AFM that the backbones remain intact, and the film is greatly compressed. It is also consistent with the observation that friction force between the tip and PDA sample is higher over the transformed region, since highly tilted and defective side-chains would expose more methylene groups to the tip, as opposed to the terminal methyl groups which have a lower surface energy.

The blue phase therefore appears to be a metastable phase. On the Langmuir trough, the high registry of the diacetylene packing permits rapid topochemical polymerization of the diyne monomers to the ene-yne conjugation upon UV illumination resulting in the blue-phase polydiacetylene. Little change in the amphiphile packing, and thus little reorientation of the alkyl side-chains, occurs. However, the hybridization change from  $sp$  to  $sp^2$  for the terminal alkyne carbons creates a stress on the polymer as a result of the  $180^\circ$  to  $120^\circ$  bond angle conversion (see figure 3). With initial UV illumination to create the blue form, significant molecular stress is built into the film. At higher degrees of polymerization, or with the application of mechanical stress or heat, the film's original structure breaks down as the alkyl chains of the blue-phase polymer reorganize to accommodate the bond angle conversion. In the case of UV polymerization or heating, this yields a closer packing (film contraction) and reorientation (vertical height increase) of the alkyl chains. In the case of mechanochromism, however, this leads to a totally different collapsed film structure.

These reorganizations, although thermodynamically more stable, produce a reduction in the effective  $\pi$ -conjugation length and result in the red form of the polydiacetylene. These results are consistent with recent NMR investigations by Lee *et al* [15] which show that the blue-to-red thermochromic transition in other PDA bulk samples involves a release of mechanical strain on the backbone and reorganization of the side-groups. Furthermore, FTIR data of Lio *et al* [12] and  $^{13}\text{C}$  NMR data of Tanaka *et al* [39] suggest that some of the tilted side-chains rotate toward the surface normal in the red phase for thermochromic films. Theoretical calculations indicate that a rotation of only a few degrees about this bond dramatically changes the  $\pi$ -orbital overlap [33], causing a significant blue-shift of the absorption spectrum. Recent molecular modelling studies [52] of PDA oligomers also show that a loss of backbone planarity leads to shifts in absorption spectra corresponding to the blue-to-red transition.

### 3.5. Thermochromism

We have also studied thermochromism in our Langmuir films, specifically, the onset of changes in the absorption spectrum and the onset of fluorescence in the trilayer poly(I) films as it was heated [14].

Thermochromic transitions of the poly-PCDA film were measured by ellipsometry and fluorescence on a film initially prepared in the blue form. The sample was annealed at a fixed temperature, and the measurement (ellipsometric or fluorescence) was acquired at that temperature. The sample was then quenched to 293 K, where a room temperature measurement was acquired. Subsequent heat-quench cycles were obtained at increments of  $5^\circ$ . The room-temperature spectra demonstrate that the major absorption feature of the blue form at 640 nm disappears and the red-form absorption features at 550 and 500 nm appear as the annealing temperature increases. At intermediate annealing temperatures, the 640 nm feature appears to shift to a shorter wavelength, resulting in an apparent new broad absorption feature at 600 nm. This feature is only observed at elevated temperatures and is not present in measurements made at room temperature either before or after annealing. Furthermore, it is only observed upon

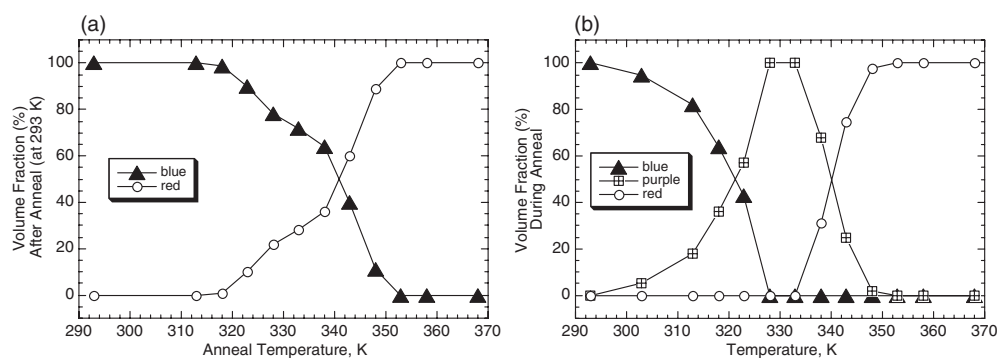


**Figure 7.** (a) Volume fractions of blue and red forms at room temperature after annealing to the indicated temperature. (b) 'Effective' volume fractions of blue-, purple-, and red-form poly-PCDA in the film at the anneal temperature.

annealing a film originally in the blue form. Material exhibiting this absorption feature we call the 'purple' form of the material. Deckert *et al* [53, 54] have postulated the existence of an intermediate 'purple' form based on kinetic aspects of the blue-to-red transition.

We can model the relative concentrations of blue and red forms by assuming that the sample consists solely of blue form at the start of the annealing study, and solely of the thermochromic red form after annealing to 368 K. Then considering the film to be made up of a mixture of blue and red forms *at room temperature* after each annealing cycle, we construct an effective index of refraction for the film using the Bruggeman effective medium approximation (EMA) [55]. The resulting volume fractions are shown in figure 7(a). Starting at about 320 K, a significant fraction of the blue form is converted to red, with near-complete conversion after annealing to 353 K.

Absorption spectra derived *at* each annealing temperature between 320 and 350 K indicate the shift of the blue absorption feature to the 'purple form'. Assuming this to be a distinct form of the poly-PCDA, and that all blue form has been converted to purple at 328 K (where the purple feature is maximized), we apply a three-component EMA analysis to the spectra. This gives the volume fractions of blue, purple, and red forms *at the annealing temperatures*. The result is shown in figure 7(b). Examination of figures 7(a) and (b) shows that the purple form reverts primarily to blue after quenching to room temperature, with approximately 30% converting to red after annealing to 330–340 K and then quenching to room temperature.

The observed threshold temperatures of  $\sim 320$  K to initiate creation of red poly-PCDA, and 353 K to establish nearly complete conversion to the red form, is similar to previous studies of other poly-PCDA films [12, 53, 56]. Collectively, these studies, along with ours, indicate that the optical properties of poly-PCDA films can be reversibly altered by heating up to approximately 320 K. Overall this change is far less profound than the changes that occur with full conversion to the red form, which occurs at  $\sim 353$  K in our film.

The purple form appears over the temperature range of 313–343 K, and its appearance at these elevated temperatures is primarily associated with the disappearance of the blue form. Inspection of figure 3(b) show that the purple absorption feature reaches its maximum intensity at about 330 K, while the blue absorption at 640 nm has largely disappeared. However, upon quenching to room temperature the blue form reappears and is still the predominant component of the film. We see no evidence for existence of the purple form at room temperature after any annealing step. The absorption maximum of the purple form shifts to shorter wavelength as the temperature increases with no apparent isosbestic point associated with the colour transition. Since the purple form exists only at elevated temperature, it appears to be a metastable form

that is interconvertible with the blue form. We also observe that, unlike the red form, neither the blue nor the purple form exhibit significant fluorescence emission.

These results lead us to propose that the purple form is a thermally distorted configuration of the blue form exhibiting a substantial shift of the absorption spectrum to shorter wavelengths. The purple form may represent a transition state in the conversion to the red form. However, our results indicate that it is energetically favourable for the purple form to revert to the blue, suggesting that the true transition state lies somewhat higher in energy and further along the reaction coordinate toward the red form. This conclusion is supported by the fact that no reversible behaviour is seen in these films once they have been converted to the red form; annealing red films does not result in appearance of the purple form, nor conversion back to the blue form. One hypothesis for the structure of the purple form may be that enhanced thermal fluctuations of the pendant alkyl side-chains occurs, and this affects the net packing density. This leads to a partial relaxation of the strained polymer backbone and a corresponding optical shift, which then disappears when the temperature is again reduced.

We have carried out first-order kinetic simulations to determine the reaction scheme by which the blue form converts to the red. Our data support a simple, first-order, irreversible transition from blue/purple to red ( $B \rightarrow R$ ) for this film, where the purple form is simply thermally distorted blue material, involving a substantial shift in the absorption spectrum. A reaction scheme involving an independent purple phase produced via a significant structural transition involving energetic barriers between blue and purple forms is not consistent with our data.

Fluorescence studies establish that only the red form of poly-PCDA displays strong fluorescence. This is a general property of PDA materials, be they thin films, bulk samples, or solutions. We can then obtain kinetic information for the irreversible transition to the red form by examining time-resolved measurements of fluorescence emission. Assuming first-order kinetics at fixed temperature, the amount of red [R] poly-PCDA is determined by  $[R]/[R_{\max}] = 1 - e^{-kt}$  where  $[R_{\max}]$  is the final amount of red poly-PCDA. Figure 8(a) shows a typical plot of fluorescence intensity versus time, in this case at 350 K, with a least-squares fit of the above equation. The rate constant at a fixed temperature  $T$  is given by  $k = Ae^{-E/RT}$  where  $E$  is the energy barrier,  $R = 1.9 \times 10^{-3} \text{ kcal mol}^{-1} \text{ K}^{-1}$  and  $A$  is the pre-exponential factor. Therefore, the slope of an Arrhenius plot [ $\ln(k)$  versus  $1/RT$ ] will be the energy barrier  $E$ . The result is plotted in figure 8(b). The linear behaviour confirms that first-order kinetics provides an accurate description of this system. From the Arrhenius plot we determine  $E = 17.6 \pm 1.1 \text{ kcal mol}^{-1}$ . This result is somewhat lower than previous measurements [53, 54] for multilayer films of PCDA  $\text{Cd}^{2+}$  salts. The fact that our films are only three layers thick, lack metal ion complexation, and are deposited on extremely flat substrates may affect the kinetics and energetics of the transition significantly. In particular, our film is likely to exhibit fewer defects and stronger thermal coupling between and within layers due to their crystallinity and structural registry, thereby reducing the energy barrier.

We have also studied the temperature dependence of the fluorescence of the stable thermochromic red form. The fluorescence intensity of thermochromic red films is strongly diminished at elevated temperatures (figure 8(c)). Yet, according to the ellipsometric measurements, these films maintain their characteristic red absorption spectrum at elevated temperatures. This effect is reversible, as the fluorescence emission recovers after quenching to room temperature. Furthermore, *cooling* the sample below room temperature leads to an *increase* in fluorescence emission. Thus, fluorescence emission for red films has a completely reversible and distinct temperature dependence.

The decrease in fluorescence emission from red films at elevated temperature is not accompanied by a similar decrease in absorption, according to ellipsometric measurements.

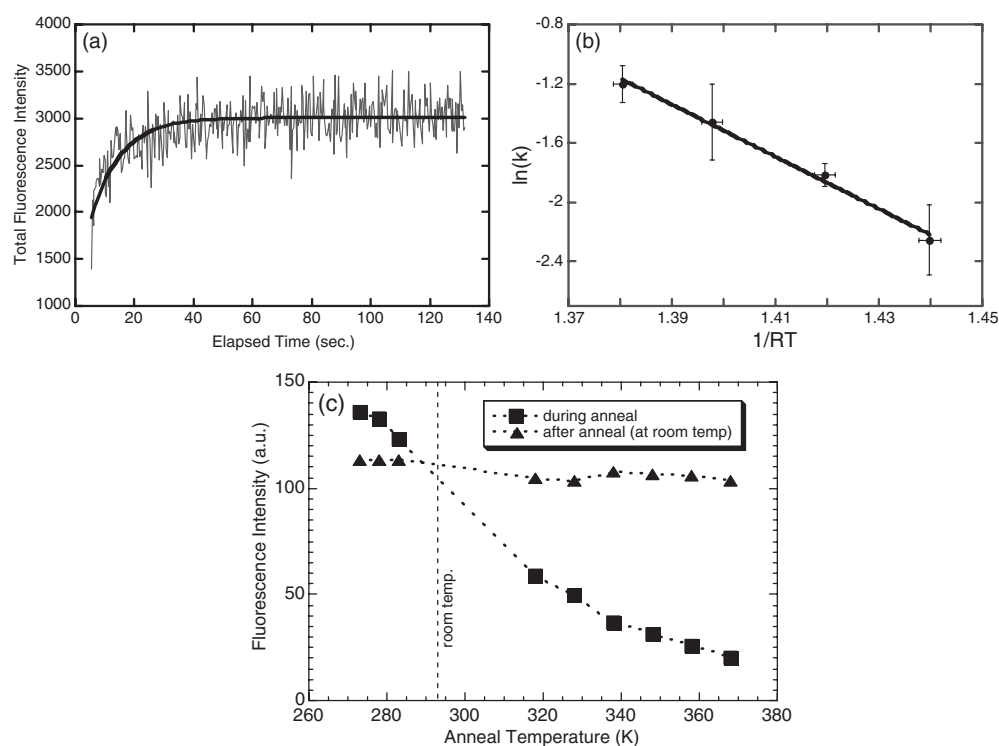


**Figure 8.** (a) Plot of fluorescence versus time at 350 K (circles) with a least-squares fit of equation (1) (solid curve). The fit provides a value of  $k$  for each measurement. (b) Arrhenius plot ( $\ln(k)$  versus  $1/RT$ ) of several measurements of fluorescence versus time such as in (a). (c) Fluorescence emission intensity versus temperature for a sample initially in the red form. Squares—intensity at the annealing temperature. Triangles—intensity at room temperature after annealing to the indicated temperature. The emission at room temperature is unaffected by the annealing cycles. Increased temperature reduces fluorescence emission, and cooling below room temperature increases fluorescence emission.

Therefore, the fluorescence emission must be reduced by a substantial enhancement of non-radiative decay processes, as opposed to changes in the absorption characteristics. Mino *et al* [56] have observed significant thermal fluctuations of the side chains of a blue film when annealed above 323 K which lead to a disordered film structure at elevated temperatures. Recent evidence suggests that the thermochromic red form is in fact *more* ordered than the blue form at room temperature, at least for trilayer poly-PCDA films, based on IR and AFM measurements [12]. Several factors therefore suggest a general correlation between side-chain ordering and fluorescence emission.

The above results indicate that we can expect significant fluctuations of the side-chains, and presumably the backbones to which they are attached, at elevated temperatures. Furthermore, these thermally induced molecular fluctuations lead to a reduction of molecular order at elevated temperatures. Both of these factors may enhance non-radiative de-excitation pathways. If so, we would then expect that cooling a photochromic red film would increase the fluorescence emission. This is indeed what we observe in figure 8(c). The significant thermal fluctuations of the alkyl side-chains at elevated temperatures are also consistent with the aforementioned hypothesis that the purple form occurs because alkyl side-chain motion allows temporary relaxation of the strained polymer backbone. Further studies of the vibration and emission

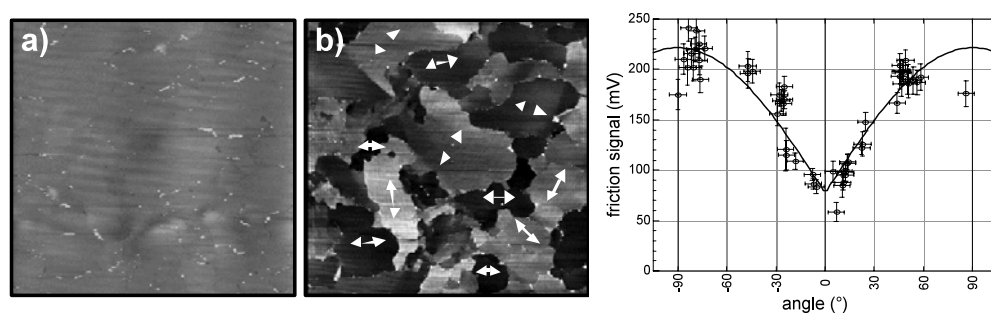


**Figure 9.** (a)  $50 \times 50 \mu\text{m}^2$  AFM topography image of a red poly(I) monolayer. (b) Simultaneous friction image. The friction image reveals the different domains. White arrows indicate the domain orientation. (c) Friction force (raw signal units) versus angle.  $0^\circ$  indicates sliding parallel to the backbone direction. The standard deviation is used for the friction error bars. The solid curve represents the fit of equation (1) to the data.

spectra of these films as a function of temperature are required to investigate this hypothesis more rigorously.

### 3.6. Friction anisotropy

AFM measurements demonstrate that the films possess strong friction anisotropy [21]. For example, measurements on the red poly(II) monolayer (figures 9(a) and (b)) reveal a domain structure. The friction force varies substantially from one domain to the next, and is nearly uniform within each domain. The topographic image reveals an essentially flat film. As mentioned above, topographic images within a single domain reveal parallel striations of varying width and uniform direction (figure 6). These striations are associated with the direction of the underlying polymer backbone, and allow us to determine the relative angle between the sliding direction and the backbone direction.

By measuring the friction force at the same load for different orientations, we find that friction is lowest when sliding parallel to the backbones, and 2.9 times larger when sliding perpendicularly (figure 9(c)). This dramatic effect may be due to anisotropic film stiffness caused by anisotropic packing and/or ordering of the alkyl side-chains, as well as the anisotropic stiffness of the polymer backbone structure itself. Along the backbone direction, the conjugated polymer bonds provide a rigid link between alkyl chains (figure 1). However, the spacing between alkyl chains linked to *neighbouring* backbones is determined by weaker interchain van der Waals' forces and head-group–substrate interactions. In other words, the lack of covalent bonding between neighbouring polymer chains allows some freedom in their spacing, consistent with previous studies of a similar PDA film [12]. Variations in film density would also explain the typical film height contrast of  $\sim 2 \text{ \AA}$  due to the striations observed in figure 6 [57].

A simple model for a scalar in-plane anisotropic tip–sample interaction force  $F_{\text{in-plane}}$  is an isotropic dissipative force  $F_1$ , plus an anisotropic term that varies as  $\sin(\theta)$  with maximum value  $F_2$ :

$$F_{\text{in-plane}} = F_1 + F_2|\sin(\theta)| \quad (1)$$

where  $\theta$  represents the domain orientation. The anisotropic term is consistent with the notion that the frictional work done is equal to the vector dot product of the distance travelled and a force that only acts perpendicular to the backbones. The absolute value is used to ensure



that this contribution is positive. Equation (1) provides a consistent fit to the data as shown in figure 9(c), giving  $F_1 \propto 77$  mV and  $F_2 \propto 144$  mV (the proportional sign is used because the data are given as uncalibrated raw signal units). Thus, according to the fit, the total friction anisotropy is  $\frac{F_{\max}}{F_{\min}} = \frac{F_1 + F_2}{F_1} = 2.9$ .

The anisotropic contribution  $F_2$  may have several sources. Lower stiffness along the perpendicular direction may lead to larger molecular deformation when sliding in that direction, and thus a larger contact area, more Gauche defect creation, and more bending of the hydrocarbon chains. These would all contribute to larger friction forces [58].

### 3.7. Imaging in-plane anisotropy with intermittent-contact AFM

The high in-plane anisotropy of the PDA films affords us an opportunity to re-examine commonly held assumptions about scanning probe measurements, such as IC-AFM [59, 60]. In IC-AFM, the AFM cantilever is driven at or near its resonance frequency so that the tip oscillates with respect to the substrate. The tip interacts strongly with the sample for a small portion of its cycle, and the reduced amplitude that results is used as a feedback signal to map out the topography of the sample. The corresponding phase shift between the drive and response is monitored simultaneously, and is generally considered to be a map of dissipation during compression of the sample along the sample normal.

Figure 10(a) shows an IC-AFM topographic image of a PCEA monolayer film with large domains [60]. Islands of extra PCEA layers are also visible. As with contact-mode AFM, each domain can be identified in the phase image by the orientation of the striations along which the PDA backbones lie [12, 23]. The typical phase  $\phi$  in figure 10(b) is approximately  $116^\circ$ . Given that the properties of PDA films *normal* to the substrate are highly uniform between domains, it is surprising that the phase  $\phi$  differs from domain to domain by up to  $2^\circ$  in figure 10(b). The maximum phase  $\phi_{\max}$  occurs when the long axis of the cantilever is parallel to the striations ( $\theta = 0^\circ$ ).

Phase shifts in IC-AFM indicate energy loss [61]. When the tip's motion is sinusoidal, the power dissipated due to the tip-sample interaction is [61, 62]

$$\bar{P}_{\text{tip}} = \frac{1}{2} \frac{k A^2 \omega_0}{Q} \left( \frac{A_0}{A} \sin(\phi) - 1 \right) \quad (2)$$

where  $\phi$  is the phase of the oscillation relative to the drive,  $k$  is the spring constant of the cantilever,  $\omega_0$  is the cantilever's resonance frequency,  $Q$  is the quality factor of the cantilever,  $A_0$  is the free oscillation amplitude of the lever, and  $A$  is the reduced amplitude during measurement. We have shown that, consistent with many IC-AFM measurements, the tip motion is very nearly sinusoidal in our experiments [60].

From figure 10(b) and equation (2), we find that the power dissipated is smallest (i.e. phase shift largest) when the striations are parallel to the long axis of the cantilever. In fact, the cantilever loses an extra amount of energy  $\Delta E \approx 2.4$  eV/cycle in domains where the striations are perpendicular, rather than parallel, to the long axis of the cantilever. The effect observed in figure 10(b) can now be explained by considering the fact that the cantilever is tilted along its long axis ( $11^\circ$  in our case). Therefore, there will be a small but significant component of tip motion parallel to the sample during each oscillation cycle. The direction of larger dissipation corresponds, as we would expect, to the direction of high friction for this component of in-plane sliding. The amount of extra energy dissipated is roughly 10% of the total energy dissipated through the tip-sample interaction. That this level of energy loss should occur due to in-plane forces is reasonable, given that the tip moves in the plane of the sample a distance that is  $\sim 20\%$  of the total tip displacement.

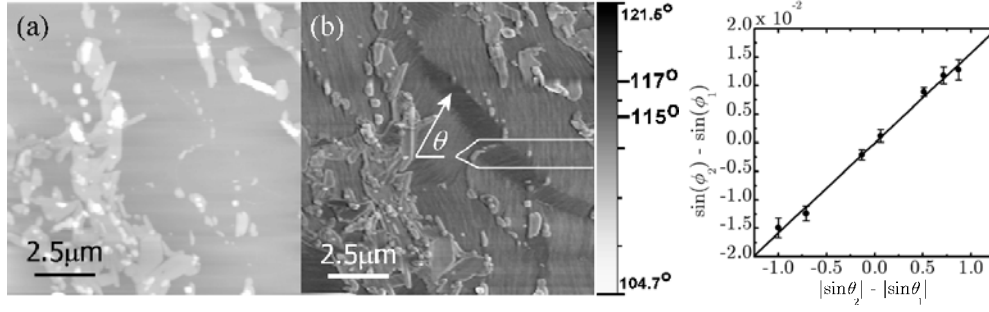


**Figure 10.** Topographic (a) and phase (b) images of a PDA monolayer thin film on mica.  $\theta$  is the angle between the local PDA backbone striations and the long axis of the cantilever. The orientation of the cantilever is sketched on the right. (c) The difference in the sines of the phase angles  $\phi$ , proportional to the difference in energy loss between domains, versus the difference in the absolute values of the sines of the angles  $\theta$ , proportional to the difference in the in-plane tip-sample dissipative forces.

Figure 10(c) is a plot of  $\Delta \sin(\phi)$  versus  $\Delta|\sin \theta|$  for the data in figure 10(b) [60]. Remarkably, we find that  $\Delta \sin(\phi)$  is proportional to  $\Delta|\sin \theta|$ , with proportionality constant  $\alpha = (1.58 \pm 0.05) \times 10^{-2}$ . This linear proportionality is discussed in detail in [60]. If equation (2) describes the power dissipation, the observed proportionality is expected. From equation (2), the difference in  $F_{\text{in-plane}}$  between two domains 1 and 2 is simply proportional to  $\Delta|\sin(\theta)| \equiv |\sin(\theta_2)| - |\sin(\theta_1)|$ . The difference in power dissipated between two domains is proportional to  $\Delta \sin(\phi) \equiv \sin(\phi_2) - \sin(\phi_1)$ , if we assume that equation (1) correctly describes the in-plane dissipation. We therefore conclude that the anisotropic forces in our experiment arise from friction, or, in addition, inelastic shear deformation. Recently we have made direct measurements of tapping mode phase as a function of the angle between the cantilever and the surface. These measurements show that—at least in the ‘attractive’ regime where contact is avoided—the more grazing the tip-sample contact, the closer the phase is to  $90^\circ$ . Thus, phase dependence on in-plane motion is a universal phenomenon, one which is easily observed in highly anisotropic, yet highly homogenous samples.

We have constructed a model which, unlike previous models of IC-AFM, takes the tilt of the cantilever into account. The model assumes Hertzian tip-sample contact, with both in-plane and out-of-plane dissipative components [60]. The key result is that components of motion both normal and parallel to the sample occur, and therefore in-plane dissipative processes can cause phase shifts. Using parameters appropriate for our system, we solve for the steady state motion of the tip. The model indicates a maximum tip-sample in-plane tip motion of  $\delta = 49.9 \pm 0.1$  pm parallel to the sample. The distance  $\delta$  is extremely small, and it is difficult to make firm distinctions between friction and shear deformation at such a small scale, as discussed below. The important result is that  $\delta$  is virtually independent of the in-plane damping. Furthermore, the model produces a nearly sinusoidal tip motion, indicating that equation (2) remains valid for the tilted-cantilever geometry.

In principle, modelling can be used to quantitatively associate the measured phase shifts with the dissipative in-plane properties of the material being imaged. These properties are friction (as quantified by the interfacial shear strength  $\tau$  between the tip and sample) [58] and dissipative shear deformation (due to viscoelasticity of the sample, as quantified by the loss tangent of the material,  $\tan \Delta$ ) [63]. Both of these mechanisms contribute to the observed dissipation and so we cannot explicitly separate them in our data. However, we can use our data to determine the upper limits of  $\tau$  and  $\tan \Delta$  by finding the values that result when attributing

all the dissipation to each mechanism respectively. The current difficulty with this approach is that the phase shifts predicted by our Hertzian model have the opposite sign to the phase shifts we observe. The reason for this discrepancy is that we have ignored adhesion in our model. Preliminary results from modelling that includes adhesion show that the phase shift changes sign and becomes consistent with our data [64].

#### 4. Conclusions

We have produced high-quality ultrathin PDA films using a horizontal Langmuir deposition technique. The number of stable layers in the film is controlled by altering the head-group functionality. The films exhibit strong friction anisotropy that is correlated with the direction of the polymer backbone structure. Shear forces applied by AFM or NSOM tips locally induce the blue-to-red chromatic transition in the PDA films.

We have shown that spectroscopic ellipsometry can be used to monitor thermochromism in ultrathin poly(diacetylene) films. Spectroscopic ellipsometry reveals that trilayer films of poly-PCDA exhibit a partially reversible transition from the blue form to an intermediate purple form, followed by an irreversible transition to the red form. The purple form appears to be thermally distorted blue material. The purple form is present only at elevated temperatures and exhibits a large, reversible shift in the absorption spectrum to shorter wavelengths. Only the red form exhibits significant fluorescence emission. From time-resolved fluorescence experiments we determine an energy barrier of  $17.6 \pm 1.1$  kcal mol<sup>-1</sup> for the irreversible transition from blue/purple to red forms.

Monolayer films of PCEA exhibit strong threefold friction anisotropy. Friction is highest when scanning perpendicular to the polymer backbone direction. We propose that this effect results from anisotropic film deformation modes.

The highly anisotropic nature of PDA films allows us to show that in-plane properties of materials can be observed using IC-AFM. This is due to the tilt of the AFM cantilever which produces a small but significant in-plane component to the tip's motion. In the case of PDA monolayers, in-plane friction and shear deformation anisotropy leads to contrast in the IC-AFM phase image. The results can be explained using a simple model that incorporates Hertzian contact mechanics with in-plane dissipation, and may be generalized to the study of other anisotropic materials.

In summary, we have demonstrated that Langmuir films of PDAs exhibit many attractive properties, and shown that numerous techniques, particularly scanning probe microscopy, can provide new insights into these properties at the nanometre scale. The coupling between mechanical, structural, and optical properties is particularly striking. These results provide further motivation for studying the synthesis and characterization of such films, and developing applications that exploit the novel anisotropic and environmentally sensitive properties of these materials.

#### Acknowledgments

We acknowledge funding from the NSF CAREER programme, grant nos DMR0094063 (MAE) and CMS0134571 (RWC), the Research Corporation (MAE), the NSF MRSEC programme, grant no DMR0079983, and the University of Wisconsin—Madison and the Army Research Office, grant no DAAD19-03-1-0102 (RWC and MAE). Some images in this paper were prepared using WSxM freeware from Nanotech Electronica. We gratefully acknowledge Tom Mayer's participation with the ellipsometric measurements. Sandia is a multiprogramme

laboratory operated by Sandia Corporation, a Lockheed Martin Company, for the United States Department of Energy under contract DE-AC04-94AL85000.

## References

- [1] Charych D H, Nagy J O, Spevak W and Bednarski M D 1993 *Science* **261** 585
- [2] Reichert A, Nagy J O, Spevak W and Charych D 1995 *J. Am. Chem. Soc.* **117** 829
- [3] Charych D *et al* 1996 *Chem. Biol.* **3** 113
- [4] Eddington D T, Liu R H, Moore J S and Beebe D J 2001 *Lab on a Chip* **1** 96
- [5] Albrecht T R, Akamine S, Carver T E and Quate C F 1990 *J. Vac. Sci. Technol. A* **8** 3386
- [6] Bloor D and Chance R R 1985 *Polydiacetylenes: Synthesis, Structure, and Electronic Properties* (Dordrecht: Martinus Nijhoff)
- [7] Day D, Hub H H and Ringsdorf H 1979 *Isr. J. Chem.* **18** 325
- [8] Tieke B, Lieser G and Wegner G 1979 *J. Polym. Sci. A* **17** 1631
- [9] Olmsted J and Strand M 1983 *J. Phys. Chem.* **87** 4790
- [10] Carpick R W, Sasaki D Y and Burns A R 2000 *Langmuir* **16** 1270
- [11] Wenzel M and Atkinson G H 1989 *J. Am. Chem. Soc.* **111** 6123
- [12] Lio A, Reichert A, Ahn D J, Nagy J O, Salmeron M and Charych D H 1997 *Langmuir* **13** 6524
- [13] Chance R R, Baughman R H, Muller H and Eckhardt C J 1977 *J. Chem. Phys.* **67** 3616
- [14] Carpick R W, Mayer T M, Sasaki D Y and Burns A R 2000 *Langmuir* **16** 4639
- [15] Lee D C, Sahoo S K, Cholli A L and Sandman D J 2002 *Macromolecules* **35** 4347
- [16] Muller H and Eckhardt C J 1978 *Mol. Cryst. Liq. Cryst.* **45** 313
- [17] Nallicheri R A and Rubner M F 1991 *Macromolecules* **24** 517
- [18] Tomioka Y, Tanaka N and Imazeki S 1989 *J. Chem. Phys.* **91** 5694
- [19] Cheng Q and Stevens R C 1998 *Langmuir* **14** 1974
- [20] Jonas U, Shah K, Norvez S and Charych D H 1999 *J. Am. Chem. Soc.* **121** 4580
- [21] Carpick R W, Sasaki D Y and Burns A R 1999 *Tribol. Lett.* **7** 79
- [22] Spevak W, Nagy J O and Charych D H 1995 *Adv. Mater.* **7** 85
- [23] Sasaki D Y, Carpick R W and Burns A R 2000 *J. Colloid Interface Sci.* **229** 490
- [24] Mowery M D and Evans C E 1997 *Tetrahedron Lett.* **38** 11
- [25] Mowery M D, Menzel H, Cai M and Evans C E 1998 *Langmuir* **14** 5594
- [26] Lu Y *et al* 2001 *Nature* **410** 913
- [27] Kobayashi T 1993 *Optoelectron. Devices Technol.* **8** 309
- [28] Hoofman R J O M, Siebbeles L D A, de Haas M P, Hummel A and Bloor D 1998 *J. Chem. Phys.* **109** 1885
- [29] Soos Z G, Galvao D G and Etemad S 1994 *Adv. Mater.* **6** 280
- [30] Eckhardt H, Eckhardt C J and Yee K C 1979 *J. Chem. Phys.* **70** 5498
- [31] Bässler H, Sixl H and Enkelmann V 1984 *Advances in Polymer Science* ed H-J Cantow (Berlin: Springer)
- [32] Sandman D J 1994 *Trends Polym. Sci.* **2** 44
- [33] Orchard B J and Tripathy S K 1986 *Macromolecules* **19** 1844
- [34] Eckhardt H, Boudreaux D S and Chance R R 1986 *J. Chem. Phys.* **85** 4116
- [35] Hankin S H W, Downey M J and Sandman D J 1992 *Polymer* **33** 5098
- [36] Ulman A 1996 *Chem. Rev.* **96** 1533
- [37] Ulman A 1991 *Introduction to Ultrathin Organic Films from Langmuir–Blodgett to Self-Assembly* (New York: Academic)
- [38] Dobrosavljevic V and Stratt R M 1987 *Phys. Rev. B* **35** 2781
- [39] Tanaka H, Gomez M A, Tonelli A E and Thakur M 1989 *Macromolecules* **22** 1208
- [40] Cholli A L and Sandman D J 1999 *Bull. Mater. Sci.* **22** 691
- [41] Rubner M F, Sandman D J and Velazquez C 1987 *Macromolecules* **20** 1296
- [42] Mowery M D and Evans C E 1997 *J. Phys. Chem. B* **101** 8513
- [43] Fuks-Janczarek I *et al* 2002 *Opt. Commun.* **209** 461
- [44] Thakur M and Krol D M 1990 *Appl. Phys. Lett.* **56** 1213
- [45] Bader M A and Marowsky G 2001 *Synth. Met.* **124** 141
- [46] Pender W A *et al* 1995 *Appl. Phys. Lett.* **66** 786
- [47] Smolyaninov I I, Zayats A V, Gungor A and Davis C C 2002 *Phys. Rev. Lett.* **88** 187402/1
- [48] Thongpin C, Young R J, Stanford J L and Lovell P A 1996 *Proc. 7th European Conf. on Composite Materials* vol 2 p 41
- [49] Day R J, Zakikhani M, Young R J and Robinson I M 1988 *Proc. SPIE—Int. Soc. Opt. Eng.* **918** 94

- 
- [50] Mowery M D, Smith A C and Evans C E 2000 *Langmuir* **16** 5998
  - [51] Burns A R, Houston J E, Carpick R W and Michalske T A 1999 *Langmuir* **15** 2922
  - [52] Burns A R, Carpick R W, Sasaki D Y, Shelnutt J A and Haddad R 2001 *Tribol. Lett.* **10** 89
  - [53] Deckert A A, Fallon L, Kiernan L, Cashin C, Perrone A and Encalarde T 1994 *Langmuir* **10** 1948
  - [54] Deckert A A, Horne J C, Valentine B, Kiernan L and Fallon L 1995 *Langmuir* **11** 643
  - [55] Bruggeman D A G 1935 *Ann. Phys.* **24** 636
  - [56] Mino N, Tamura H and Ogawa K 1991 *Langmuir* **7** 2336
  - [57] Fenter P, Eisenberger P and Liang K S 1993 *Phys. Rev. Lett.* **70** 2447
  - [58] Carpick R W and Salmeron M 1997 *Chem. Rev.* **97** 1163
  - [59] Marcus M S, Eriksson M A, Sasaki D Y and Carpick R W 2003 *Ultramicroscopy* **97** 145
  - [60] Marcus M S, Carpick R W, Sasaki D Y and Eriksson M A 2002 *Phys. Rev. Lett.* **88** 226103
  - [61] Cleveland J P, Anczykowski B, Schmid A E and Elings V B 1998 *Appl. Phys. Lett.* **72** 2613
  - [62] Tamayo J and Garcia R 1997 *Appl. Phys. Lett.* **71** 2394
  - [63] Lakes R S 1999 *Viscoelastic Solids* (Boca Raton, FL: Chemical Rubber Company)
  - [64] D'Amato M J, Marcus M S, Sasaki D Y, Eriksson M A and Carpick R W 2004 *Appl. Phys. Lett.* submitted